2021-01-5106 Published 29 Nov 2021

# Impact of Microstructure and Surface Treatment on Thermal Properties of Gray Cast Iron Brake Rotors

**Rohit Jogineedi and Vishal Reddy Singireddy** Southern Illinois University Carbondale

**Sai Krishna Kancharla** Tech M3, Inc.

**Swapnil S. Salvi and Ankur Jain** University of Texas at Arlington

**Peter Filip** Southern Illinois University Carbondale

***Citation:*** Jogineedi, R., Singireddy, V.R., Kancharla, S.K., Salvi, S.S., et al., "Impact of Microstructure and Surface Treatment on Thermal Properties of Gray Cast Iron Brake Rotors," SAE Technical Paper 2021-01-5106, 2021, doi:10.4271/2021-01-5106.

## Abstract

Friction interaction between brake materials sees a rise in temperatures of over 1000°C contributing to thermal fade of brakes and deterioration/cracking of rotors. Various microstructural features like graphite, ferrite, and pearlite could influence the thermal properties and related friction performance of the brake materials. Even more relevant impact on thermal properties of rotors can be expected after coatings or surface treatments. The primary purpose of this research is to identify the impact of microstructure and surface treatment on the thermal properties of four types of gray cast irons subjected to modified (when compared to their current industrial production) manufacturing processes. These rotors were marked as A (ASTM A48, C30), B (ASTM A48, C20), C (ASTM A48, C30), and D (JIS G5501, FC150), respectively [1, 2]. Complete chemical and material characterization of the brake rotors using optical emission spectrometer (OES), carbon-sulfur combustion analyzer, laser flash apparatus, polarized light microscopy (PLM), and density (analytical balance and Archimedes principle). The gray cast iron rotors are typified for a fully pearlitic gray cast iron with about 2-4 vol.% of "free" ferrite. Graphite can be further classified as type VII-C5 of superimposed flake size and random orientation for rotors B, C, and D, and type VII-D5 of interdendritic segregation and random orientation for Rotor D. Thermal properties were recorded at room temperature (25°C) and between 50°C and 500°C, with a step size of 50°C. Thermal diffusivity and conductivities decreased with increasing temperature, while specific heat capacities increased with increasing temperature for all studied rotors. Initial mathematical models show the impact of surface treatment and graphite content to be dominant over observed thermal properties. Further scrutiny identifies the influence of applied surface treatment to be dominant over microstructure for thermal diffusivity when the combined effect of microstructure and surface treatment was studied. However, none of these factors were found to be contributing well to thermal conductivity and specific heat capacity models when the combined effect was considered.

## Keywords

Thermal, Frictional heating, Surface coating, Brake disk

## 1. Introduction

The excellent properties of gray cast irons make them a key material for producing critical automotive components like internal combustion engine blocks and brake rotors. Gray cast iron is a metal matrix composite comprising ferrite, pearlite, graphite, carbides, and nonmetallic inclusions [3, 4]. Ferrite is the $\alpha$-Fe phase with low carbon content with low strength and high ductility. Pearlite is typically comprised of alternative lamellar planes of ferrite and cementite, formed during a eutectoid transformation. However, this lamellar structure can transform to a globular structure when fully lamellar pearlitic steels are subjected to severe thermal post-treatments or are not cooled down sufficiently after pearlitic transformation [5]. Graphite is a form of carbon, commonly found as flakes that are dispersed into the matrix of a typical gray cast iron. The American Society for Testing and Materials (ASTM) A247 standard subclassifies the graphite flake morphologies into five types and eight classes [6]. Carbides are hard and brittle intermetallic compounds formed during a eutectic transformation, commonly known as cementite. However, there are other "free" carbides that are formed due to the presence of alloying elements like vanadium,

molybdenum, and so on. Nonmetallic inclusions typically include oxides, sulfides, nitrides, and phosphides, which are commonly formed due to the presence of elements from recycling scrap material. "Mean-free path," typically defined as a feature where phonons move without disruption, depends on the size and morphology of the various microstructural features identified. The foundry practices adopted can influence the volume, content, and morphology of the various microstructural features identified in a typical gray cast iron, which impacts their mechanical, chemical (corrosion), and thermal properties [7, 8, 9, 10].

Increasing spacing between graphite improves the total elongation, tensile strength, spall strength, and fracture toughness of the cast iron materials [11, 12]. As thermal diffusivity of graphite is considerably larger when compared to thermal diffusivity of ferrite and pearlite, respectively [13], it is expected that the increased spacing between graphite leads to somehow lower thermal diffusivity and thermal conductivity of gray cast irons. It was also found that the increase in the content of pearlite present in the metal matrix has a greater impact on the spall strengths compared to the increase in the content of free ferrite [12]. The mechanical strength of pearlite increases with decreased size of pearlitic grains and sub-grains as well as with decreasing interlamellar spacing between ferrite and cementite [10]. Besides this, the distribution of graphite network in the gray cast iron microstructure influences the occurrence of graphitic corrosion, where graphite acting as the cathode accelerates anodic dissolution of nearby iron, thereby decreasing the mechanical strength of gray cast iron [14].

When gray cast iron is used in a thermally challenging environment, such as in friction brakes, the morphology, quality, and quantity of these phases can change dramatically due to the resulting temperature of friction surfaces. For instance, a study conducted by S. K. Rhee et al. shows that pearlite found in cast iron rotors were transformed to martensite due to increased temperatures from friction testing [15]. Increased temperature occurring from friction between brake pads and rotors also influences the formation of wear debris and friction layers on the rubbing surfaces, which could considerably impact braking performance [16]. In this context, thermal fade has been widely reported as an unwanted phenomenon, resulting in an extremely undesirable decrease of the coefficient of friction at high temperatures [17, 18, 19, 20]. Extreme temperatures generated during the braking process could also lead to bulk material degradation, which could lead to brake failure [21]. Additional phenomena such as thermal shock, crack formation, phase transformations, and increased residual stresses in brake rotors also occur due to local heating [22].

The key thermal transport properties that govern the temperature evolution of a material include thermal conductivity $k$, specific heat capacity $C_p$, and thermal diffusivity $\alpha$. The three are related to each other as $\alpha = \frac{k}{\rho C_p}$, where $\rho$ is the specific mass. These "thermal" properties are governed particularly by the amount and the morphology of graphite flakes. The other microstructural elements such as ferrite and pearlite, which greatly depend on the chemistry and casting processes of a particular type of cast iron, influence the thermal properties of cast irons [23, 24].

The stacking of ferrite and cementite lamellae and the presence of graphite promoting alloying elements are known to contribute toward the overall thermal conductivity/diffusivity of the cast iron [13, 25, 26]. The lower volume content of the graphitic phase the larger distance between graphite flakes, their smaller size (smaller "mean free path" for phonons) are parameters leading to a lower thermal diffusivity and conductivity, respectively [23]. The type A graphite, as defined by ASTM A247 [6], when combined with greater graphite spacing helps in attaining the best thermal fatigue resistance through reduced thermal crack propagations [7]. The addition of carbide-promoting elements such as molybdenum to the bulk material also has a considerable impact on the effect of thermal shock—a mechanical load caused by rapid change of temperature about a point [27]. It is also noted that thermal diffusivity decreases with increasing temperature [23].

In addition to the microstructural influence, the application of surface treatments and coatings also exhibited a substantial impact on the thermal properties and the related tribological properties of the cast iron material. Specifically, ceramic coatings help prevent the extreme increase of the bulk temperatures by the formation of a thermal barrier, which can often be related to thermal stresses and thermal shocks, and, in this capacity, playing a vital role in preventing the bulk degradation of brake rotors. Some authors argue that this could lead to a corresponding brake emissions reduction [28], but it is not always the case, as the friction surface temperature may increase drastically, and this typically leads to increased wear of the friction counterpart. Previously reported papers [28, 29, 30, 31] on ceramic coatings such as $Al_2O_3$-Al, Yttria Stabilized Zirconia (YSZ), TiAlN, and CrN show that these coatings influence differently the thermal diffusivity of the bulk material. For instance, YSZ has been reported [28] as a thermal barrier coating to contain the heat generated in engines, whereas $Al_2O_3$-Al, TiAlN, and CrN have been shown to increase thermal diffusivity and oxidation resistance of the alloys due to the presence of Al and Cr [29, 31]. Hard metal carbides like WC and $Cr_3C_2$ when bonded with other metals, are one of the frequently used coating techniques to improve the wear resistance of brake rotors [32, 33, 34]. Besides these coatings, treatments like carbonitriding and ferritic nitrocarburizing are found to be an efficient way of altering the material properties of the base metal. Ferritic nitrocarburizing is a thermochemical diffusion process that introduces carbon and nitrogen into the surface of ferrous materials. However, most of the previous literature studies were limited in identifying their impact to improve the hardness and corrosion resistance of cast iron [35, 36, 37, 38] and have no studies showing their impact on thermal properties of cast iron. This paper along with the influence of microstructure studies the influence of a patented surface treatment process, which is a combination of bombardment of gray cast iron surfaces with heavy ions (pure forging) and simultaneous introduction of new chemical(s) to the volume adjacent to the surface [39].

A very limited number of studies are available on establishing effective mathematical models to quantify the impact of microstructure and different applied surface treatments on

the thermal properties of gray cast iron used for friction brakes. This paper focuses on establishing effective mathematical models, which can help in identifying the contribution of different microstructural elements and surface treatment applied over the thermal properties measured. To develop these models, results from an experimental investigation of thermal properties dependence on patented surface treatment and major microstructural elements identified in four types of gray cast irons were obtained from the same facility. The treated and untreated pearlitic gray cast iron rotors [1], were studied for thermal properties within a typical operating range of 25°C to 500°C. The mathematical models adopted reveal vital information in understanding the influence of microstructure and applied surface treatment over the thermal behavior of the materials studied. However, these models could further be improved by providing more statistically relevant data and help in the prediction of thermal behavior of gray cast irons being used through the microstructural and applied surface treatment information obtained.

# 2. Regression Diagnostics

The lack of a specific method to verify the correctness of a model with a large number of variables as identified in this research makes it extremely difficult to build good predictive models [40]. Residuals are calculated by subtracting the estimated response values from the actual values, i.e., $Y_i - \hat{Y}_i$, where $Y_i$ represents the actual response value and $\hat{Y}$ represents the fitted response [41]. The Breusch-Pagan test, developed by Trevor Breusch and Adrian Pagan is often used to verify the constant variance assumption [42]. An auxiliary regression equation is calculated using squared residuals of the original regression model as a response variable. The test statistic for the test, $\chi 2 = nR^2$, where $n$ is the number of observations and $R^2$ is the coefficient of determination value of the auxiliary regression equation. The $p$-value is then calculated based on test statistics and the degree of freedom of regression. The null hypothesis of the test assumes that there is constant variance in the model. If the $p$-value of the test is greater than the assumed $\alpha$ (0.05), then the null hypothesis cannot be rejected and indicates that the constant variance assumption is valid. Multicollinearity is when there is a moderate or high correlation between the predictor variables. When multicollinearity exists, the coefficients of predictors vary depending on the other predictors already in the model. This affects the reliability of the model and leads to different hypothesis test results each time. Variance Inflation Factors (VIF) are used to check for multicollinearity [43]. The VIF gives the value by which the variances are inflated. For a $k$th predictor, the VIF value is given by $\mathrm{VIF}_k = \frac{1}{1-R_k^2}$, where $R_k^2$ is the $R^2$ value obtained by regressing the $k$th predictor on another predictor variable. High VIF values indicate multicollinearity and need to be rectified. If a point or several points change the regression model significantly, they are known as influential points. It is very important to identify these points as they can be very detrimental in accepting or rejecting a model. The points in response with high standardized residuals are known as outliers. Outliers may also be present in predictors and are often referred to as high leverage points. Cook's distance is one of the very widely used methods to determine influential points [41]. The influence of an $i$th observation is given by

$$C_i = \frac{\sum_{j=1}^{n} \left(\hat{y}_j - \hat{y}_{j(i)}\right)^2}{\hat{\sigma}^2(p)}, \; i = 1,2,\ldots,n$$

where $p$ is the number of predictors, $\hat{y}_j$ is the response of full data, and $\hat{y}_{j(i)}$ is the response with the $i$th observation removed. $C_i$ values are usually examined using plots and influential points are investigated. Values greater than 1 are generally considered influential. When detecting outliers especially in large datasets, the $t$ test to detect large studentized residuals is restricted by the general threshold of $t_{1-\frac{\alpha}{2},n-p-2}$. In order to overcome this, Bonferroni correction was introduced [44]. The significance level is divided by the number of observations $n$ changing the threshold to $t_{1-\frac{\alpha}{2n},\,n-p-2}$, thereby eliminating any errors. This test is found in the car package of $R$ statistical language as an outlier test [45].

# 3. Experimental

## 3.1. Sample Preparation

For thermal property measurements, one sample of 6 mm diameter and 2 mm thickness, representing the friction surface, were cut out of each brake rotor (four untreated rotors and four treated rotors), with the help of core drilling process and surface milling performed on the untreated sides.

For chemical analysis, samples with a mass of 35 ± 1 g cut from gray cast iron castings were remelted into round chilled wafer specimens (diameter = 28 mm, thickness = 7 mm) using a Kel-Melt furnace (Kel-Melt 5420-M with TIG Torch).

To quantify the various microstructural elements found in the investigated brake rotors, rectangular samples with an approximately 10 mm × 10 mm cross section and a height of 10 mm were cut from the brake rotors. The location closely represents the cast irons' microstructure in the volume adjacent to the rotor friction surface. The samples were then molded using Buehler phenolic resin (ProbeMet Conductive Compression Mounting Compound) and Buehler SimpliMet 2 "hot press" to obtain coupons of 25.4 mm diameter and approximately 30 mm height. The coupons with molded samples were mounted on a Buehler EcoMet 3 polisher and subjected to standard metallographic preparation, starting with a 180 grit Buehler sandpaper, followed by 240, 400, 600, 800, and 1200 grit Buehler sandpapers, respectively, and finally polished using a 0.05 µm alumina slurry. Samples were flushed with water and ethyl alcohol at each stage to get rid of any debris from polishing. After studying the unetched molded samples for graphite content and morphology, the

samples were etched using a 2% Nital solution to reveal the ferrite and pearlite structure of the polished samples.

## 3.2. Chemical Analysis

The round chilled wafer specimens obtained were analyzed using an ARL 3460 optical emission spectrometer (OES) and a LECO CS744 carbon-sulfur combustion analyzer. The combustion analyzer is used to quantify the carbon content in the castings, using a small piece of 0.5 ± 0.1 g, broken from a thin slice cut from the castings. Apart from the carbon content, the round chilled wafer samples obtained from remelting are tested on an OES to quantify the other alloying elements present in the selected castings.

## 3.3. Thermal Property Measurements

A uniform graphite coating (DGF-123 Dry Graphite Film Lubricant) was sprayed on both faces to standardize the emissivity of various samples. Measurements using the laser flash method were carried out at room temperature (25°C) and from 50°C to 500°C in steps of 50°C, using the Netzsch LFA 467 instrument [46]. Sufficient time is provided to reach thermal equilibrium at each point before measurement. Thermal equilibrium was assumed to be reached when the temperature does not change by more than 1°C over a period of 30 seconds. Three flash shots were taken for each sample at each temperature, and the average of these three shots was used to determine thermal diffusivity. At each point, the flash width was adjusted by the instrument to minimize the noise in the measurements and obtain good agreement with the theoretical model. Corrections for various other aspects of the experiment, such as finite pulse width, character of the sample surface and its emissivity, and convective heat losses, are made [47].

In addition to thermal diffusivity, the specific heat capacity of the sample can be determined by comparative measurement in which the thermal response of the sample of interest is compared with that of a standard sample of well-known thermal properties. It can be shown that the peak temperature on the backside is inversely proportional to the heat capacity of the sample. Therefore, the specific heat capacity of the sample of interest can be obtained from that of the standard sample as follows:

$$C_{p,sample} = \frac{C_{p,standard} T_{max,standard}}{T_{max,sample}} \qquad \text{Eq. (1)}$$

Once thermal diffusivity and specific heat capacity are determined, thermal conductivity can be obtained easily as follows:

$$k = \alpha \cdot \rho \cdot C_P \qquad \text{Eq. (2)}$$

where $\rho$ is the mass density of the sample that can be easily measured separately.

## 3.4. Quantitative and Regression Analysis

The microstructure (graphite, ferrite, and pearlite) of polished samples obtained were analyzed using Nikon Microphot FX polarized light microscopy (PLM). Ten optical micrographs representing the overall microstructure of each polished sample were obtained for the quantitative analysis. These obtained micrographs were then analyzed using ImageJ software to quantify the average size of graphite flakes and the average volume content of graphite, ferrite, and pearlite observed.

By using the Multiple Linear Regression (MLR) analysis, the data obtained by quantitative analysis of microstructure were then correlated to the thermal property measurements using R statistical language. The general form of the models developed can be represented as $\hat{Y} = \hat{\beta}_0 + \hat{\beta}_1 X_1 + \cdots + \hat{\beta}_p X_p$ [48], where $\hat{Y}$, $\hat{\beta}_i$, and $X_i$ represent response variables (thermal diffusivity, thermal conductivity, and specific heat capacity), coefficients, and predictor (content and morphology of microstructural features identified and treatment) variables. Parameter estimation or fitting in the model correlating microstructure and thermal properties is carried out using the least-squares method. The coefficients are determined by minimizing the sum of the square of residuals, $\sum_{i=1}^{n} \varepsilon_i^2 = \sum_{i=1}^{n} \left( y_i - \beta_0 - \beta_1 x_{i1} - \cdots - \beta_p x_{ip} \right)^2$. The following four main assumptions are made for an MLR [40]:

i. Assumption on the form of the model: The response $Y$ and the predictors $X_1$, $X_2$, … $Xp$ are assumed to be linearly related. This is called linearity assumption.
ii. Assumptions on errors: Errors are assumed to be normally distributed, with a mean of zero, and are assumed to have the same variance.
iii. Assumptions about predictors: The predictor variables are assumed to be independent of each other. This is referred to as the no multicollinearity assumption.
iv. Assumptions about observations: All observations are assumed to be reliable, with an approximately equal influence on the predicted model.

Several iterations were performed to finalize the models that can predict the correlation existing between the size/volume content of microstructural elements and measured thermal properties. The obtained thermal property measurements and quantitative analysis results were also represented graphically using MATLAB R2018b.

# 4. Results and Discussions

## 4.1. Chemical Composition and Microstructure

The quantitative chemical analysis performed on the four studied rotor materials shows the carbon equivalent and contents of major alloying elements in Table 1.

**TABLE 1** Complete chemical analysis of the four studied rotor materials, quantifying the carbon equivalence and major alloying elements used.

| | Rotors | | | |
|---|---|---|---|---|
| | A | B | C | D |
| **CE** | 4.03 | 4.19 | 4.22 | 4.45 |
| **C** | 3.46 | 3.70 | 3.46 | 3.81 |
| **Si** | 1.65 | 1.43 | 2.26 | 1.90 |
| **Mn** | 0.75 | 0.45 | 0.61 | 0.52 |
| **P** | 0.06 | 0.03 | 0.03 | 0.03 |
| **S** | 0.03 | 0.07 | 0.08 | 0.07 |
| **Ni** | 0.01 | 0.06 | 0.08 | 0.07 |
| **Mo** | 0.61 | 0.03 | 0.04 | 0.02 |
| **Cr** | 0.29 | 0.12 | 0.17 | 0.14 |
| **Cu** | 0.29 | 0.17 | 0.18 | 0.15 |
| **Al** | 0.00 | 0.00 | 0.00 | 0.00 |
| **Ti** | 0.02 | 0.01 | 0.01 | 0.01 |
| **Sn** | 0.00 | 0.07 | 0.02 | 0.02 |



It is well known that the varying content of Fe, C, and other alloying elements impacts the content and morphology of microstructural elements [23, 24]. The increased content of C and Si is known to increase the content and promote the formation of flake-like graphite, whereas additions of Mn, Ti, P, Cu, Cr, Ni, and Sn considerably reduce the graphite size while increasing the content of pearlite [4, 27, 49, 50]. On the other hand, alloying elements like Mo and Ni also influence the graphite content and the thermal shock resistance of the base alloy. A study reported by [27] shows that a decrease in Mo content or increase in Ni content help in improving the graphite content and thermal shock resistance of the base alloy. Al and S are usually added in controlled low amounts as inoculants to improve the overall mechanical and thermal properties of the bulk material [4].

The optical micrographs given in Figures 1(a), 1(b), 1(c), and 1(d) represent mechanically polished and unetched cross sections of selected gray cast iron rotors. The presence of graphite in the form of flakes, with varying morphology and volume content, can be easily seen in the different selected

**FIGURE 1** Typical PLM micrographs showing the graphite distribution of unetched selected gray cast iron samples, Rotor A (a), Rotor B (b), Rotor C (c), and Rotor D (d).

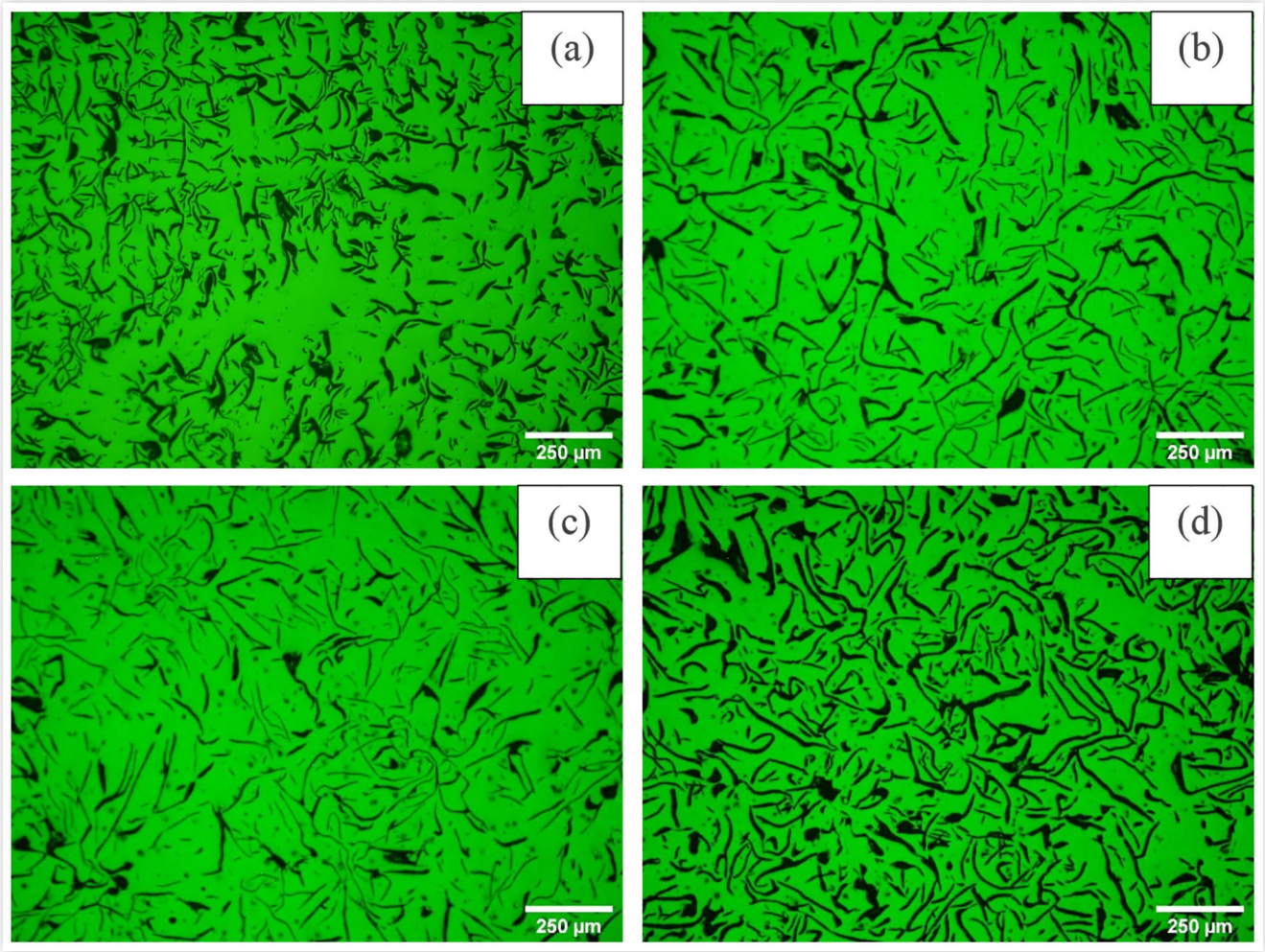

**FIGURE 2** Typical PLM micrographs showing the graphite distribution of etched selected gray cast iron samples, Rotor A (a), Rotor B (b), Rotor C (c), and Rotor D (d).

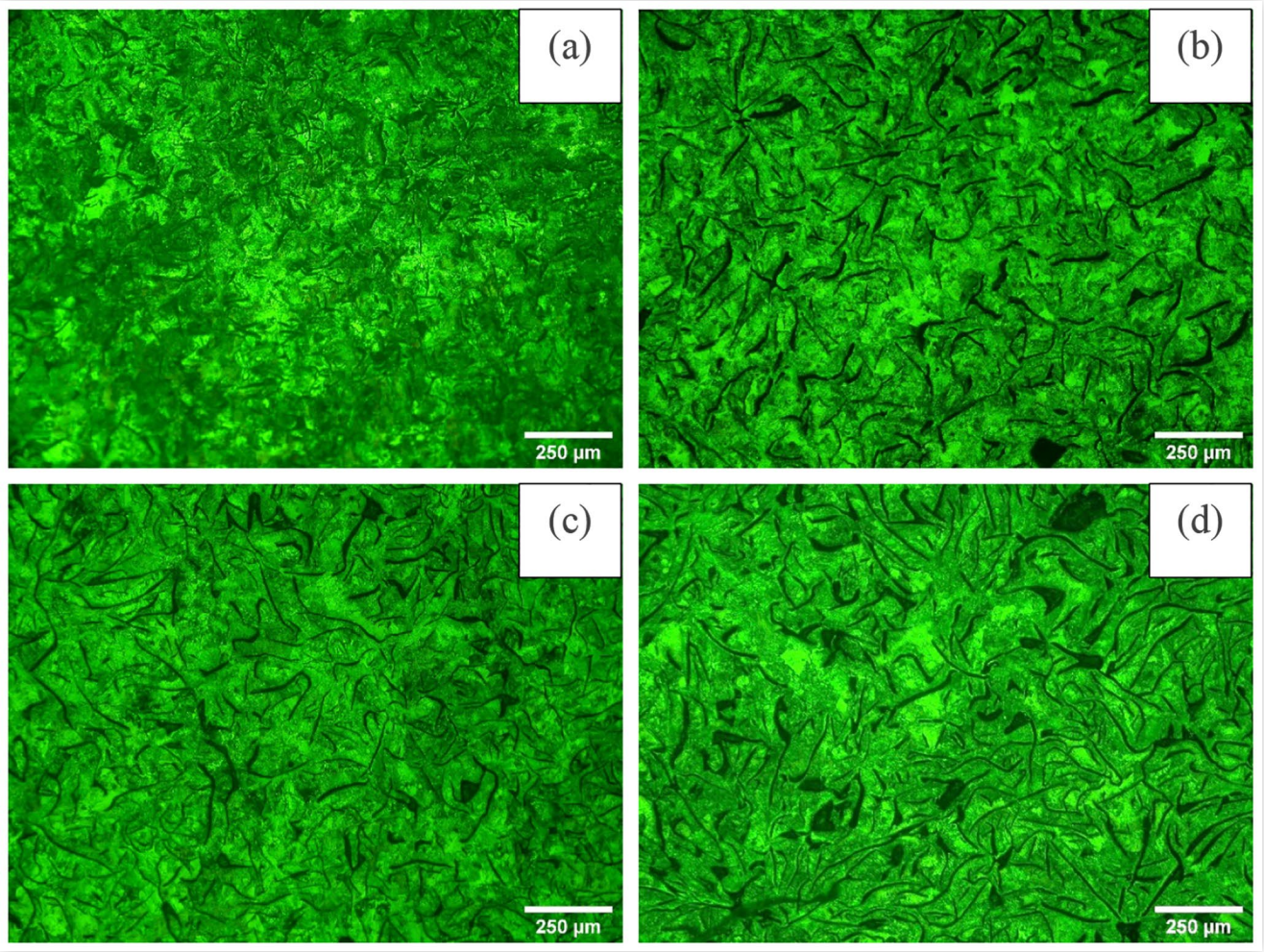




samples. The specifications given in the ASTM A247 [6] standard along with average graphite flake size obtained from the quantitative results reveal Rotor A with type VII-D5 subclassification, interdendritic segregation, and random orientation, and rotors B, C, and D with a similar type VII-C5 subclassification, superimposed flake size, and random orientation.

The selected gray cast iron samples were etched using a 2% Nital solution and examined under PLM to study the distribution and volume content of "free" ferrite and pearlite. The optical micrographs given in Figures 2(a), 2(b), 2(c), and 2(d) represent etched cross sections of selected gray cast iron rotors. These micrographs reveal fully pearlitic structure in all three selected samples with varying volume content of pearlite and "free" ferrite. The quantitative analysis obtained from ten randomly selected spots from each studied etched rotor sample reveals varying ferrite and pearlite content of rotors A, B, C, and D, as tabulated in Table 2. These results reveal nearly similar ferrite contents in rotors A and C, and B and D, respectively. Besides the ferrite content, the pearlite content observed reveals the lowest pearlite content in Rotor A with the highest graphite content and the highest pearlite content in Rotor C with the lowest graphite content. The measured volume contents of graphite, "free" ferrite, and pearlite in the selected rotors are graphically represented as given in Figure 3. The graphical representation reveals considerable differences in volume contents of graphite, "free" ferrite, and pearlite observed in the selected gray cast iron rotors.

Besides the volume content measured, the quantitative analysis results obtained unetched samples reveal varying graphite flake sizes of rotors A, B, C, and D, as tabulated in Table 3. These results do not show any reasonable correlation between the graphite content and the average graphite flake size observed. For instance, Rotor A with the highest graphite content exhibited a shorter average graphite flake size, whereas

**TABLE 2** Complete quantitative analysis of the four studied rotor materials, quantifying the content of ferrite, graphite, and pearlite.

| Rotors | Ferrite vol.% | Graphite vol.% | Pearlite vol.% |
|---|---|---|---|
| **A** | 2.4 | 25.9 | 71.7 |
| **B** | 3.7 | 18.9 | 77.4 |
| **C** | 2.5 | 16.6 | 80.9 |
| **D** | 3.8 | 22.7 | 73.5 |

**FIGURE 3** Typical graphical representation of measured volume content of graphite, "free" ferrite, and pearlite in selected gray cast iron rotors.

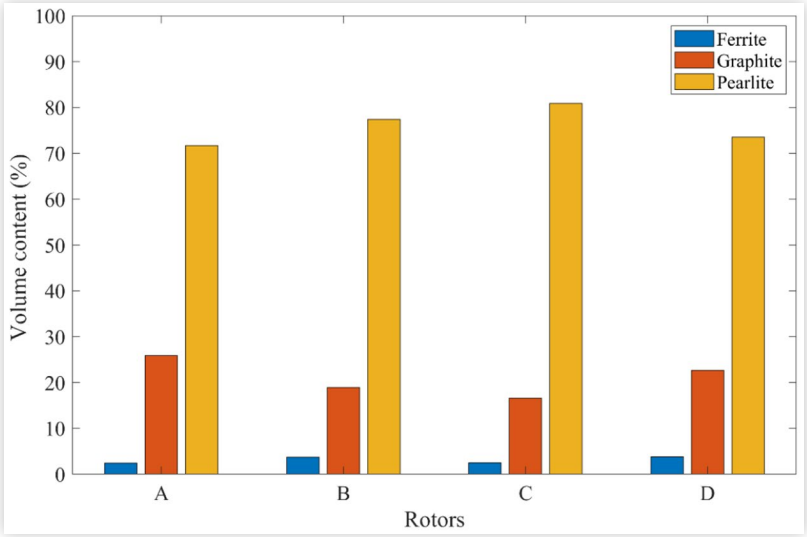




Rotor C with the lowest graphite content exhibited longer average graphite flakes when compared to Rotor A, but shorter graphite flakes when compared with rotors B and D. The statistical spread of the different graphite flakes observed from the optical micrographs obtained for each studied rotor is given in Figure 4. The plot obtained defines a considerably smaller distribution of graphite flakes in Rotor A compared to rotors B, C, and D, which represented a nearly similar and higher spread, respectively. The average and maximum graphite flake sizes measured are also plotted in Figure 4 along with the statistical spread, which also shows a similar trend, where Rotor A exhibits a shorter average and maximum graphite flake size, compared to rotors B, C, and D.

A histogram distribution of graphite flakes observed in the studied gray cast iron rotors is given in Figure 5. This distribution defines the number of graphite flakes observed in each class according to the specifications given in the ASTM A247 standard [6]. The distribution obtained reveals the presence of more graphite flakes in classes 1, 2, 3, 4, and 5 for rotors A and C, and in classes 3, 4, and 5 for rotors B and D. Despite the number of graphite flakes observed, rotors A and C, and rotors B and D, represent a nearly similar distribution of graphite flakes through classes 1 to 6, respectively, with very few graphite flakes in classes 7 and 8.

The observed slight variations in chemical composition along with the manufacturing procedures adopted had a considerable impact on the content, distribution, and morphology of graphite, ferrite, and pearlite identified in the studied alloys. The varying content, distribution, and morphology of graphite observed in the bulk material is known to influence the thermal properties as reported in [23] and shall be studied in detail in the preceding parts of the article.

**TABLE 3** Complete quantitative analysis of the four studied rotor materials, quantifying the average and maximum graphite flake size.

| Rotors | Avg. size (μm) | Max. size (μm) |
|---|---|---|
| **A** | 53.2 | 240.9 |
| **B** | 77.7 | 353.6 |
| **C** | 65 | 326.6 |
| **D** | 78.1 | 355 |



## 4.2. Thermal Properties

The measured thermal diffusivity, thermal conductivity, and specific heat capacity of studied untreated and treated rotors, at room temperature (25°C) and over a range of temperatures (50°C to 500°C, with step size 50 °C) are plotted in Figures 6(a), 6(b), and 6(c), respectively. While thermal diffusivity and thermal conductivity decrease with increasing temperature, specific heat capacity values exhibit an increase with temperature.

The measured thermal diffusivity, thermal conductivity, and specific heat capacity values of untreated and treated rotors at room temperature (25°C) and at elevated temperature (500°C) are given in Table 4. All studied rotors (untreated and treated) exhibited an approximately 50% decrease in their thermal diffusivity values when tested from 25°C to 500°C. The reduction in thermal conductivity from room temperature to 500°C is around 38% for all untreated rotors and treated rotors A, B, and C, respectively. The reduction for Rotor D—45%—is slightly larger. Rotor A exhibited the highest thermal diffusivity and conductivity, and Rotor C exhibited the lowest thermal diffusivity and conductivity among untreated rotors, with increasing temperature. Within treated rotors, Rotor D exhibited the highest thermal diffusivities and conductivities, while Rotor C still had the lowest thermal diffusivities and conductivities with increasing temperature. On an overall comparison, the treated Rotor D exhibited the highest thermal diffusivities and conductivities, and the untreated Rotor C exhibited the lowest thermal diffusivities and conductivities with increasing temperature.

**FIGURE 4** Typical boxplot representation of measured graphite flake sizes in selected gray cast iron rotors.

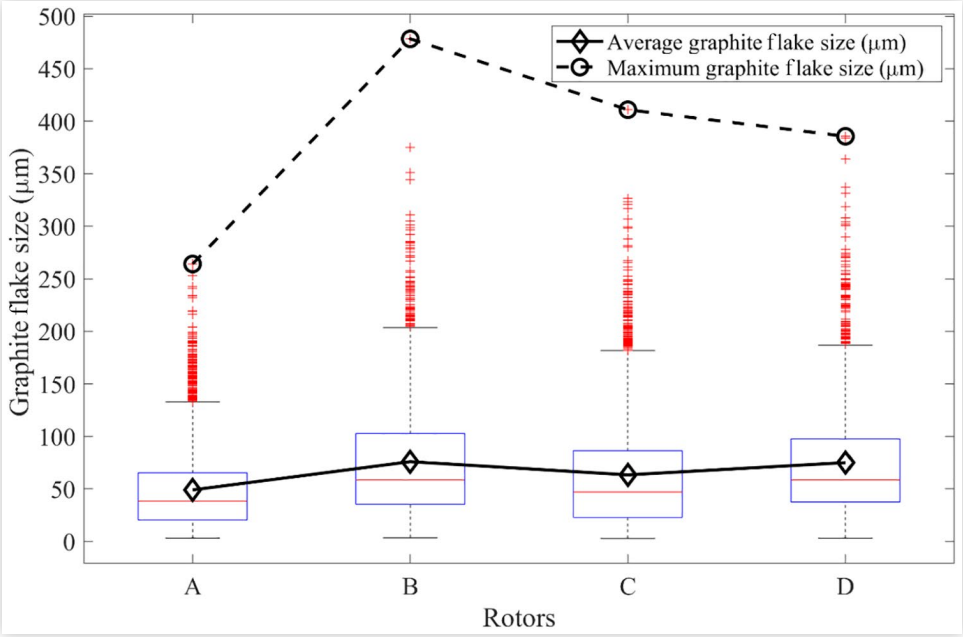


**FIGURE 5** Typical histogram distribution of measured graphite flake sizes in selected gray cast iron rotors as per the subclassification given in the ASTM A247 standard.

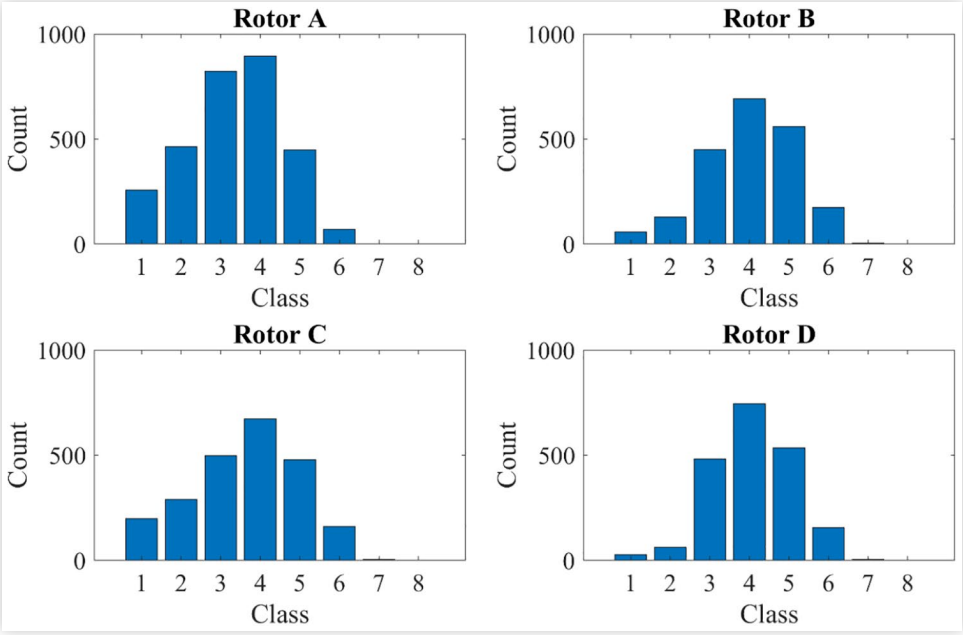


The measured specific heat capacities have seen a rise with increasing temperature, where irrespective of the treatment, rotors A, B, C, and D exhibited an approximate increase of 29%, 25%, 23%, and 25%, respectively. Rotor C exhibited the highest specific heat capacities and Rotor A exhibited the lowest specific heat capacities for untreated rotors, with increasing temperature. Whereas for treated rotors, Rotor D exhibited the highest specific heat capacity and Rotor A exhibited the lowest specific heat capacity. When all rotors were observed together, the treated Rotor D exhibited the highest specific heat capacities, and the treated Rotor A exhibited the lowest specific heat capacities, with increasing temperature.

Regardless of the type of material studied, the treatment had a significant impact on the measured thermal properties. The treatment process helped in improving the thermal diffusivities of the base alloy by approximately an average of 2.1%, 6.9%, 1.4%, and 2.8%, in rotors A, B, C, and D, respectively. However, the treatment impact on thermal conductivity and specific heat capacity was found to be inconsistent. The thermal conductivities of Rotor A were approximately

**FIGURE 6** Graphical representation of thermal properties of studied rotors, Thermal Diffusivity (a), Thermal Conductivity (b), Specific Heat Capacity (c).

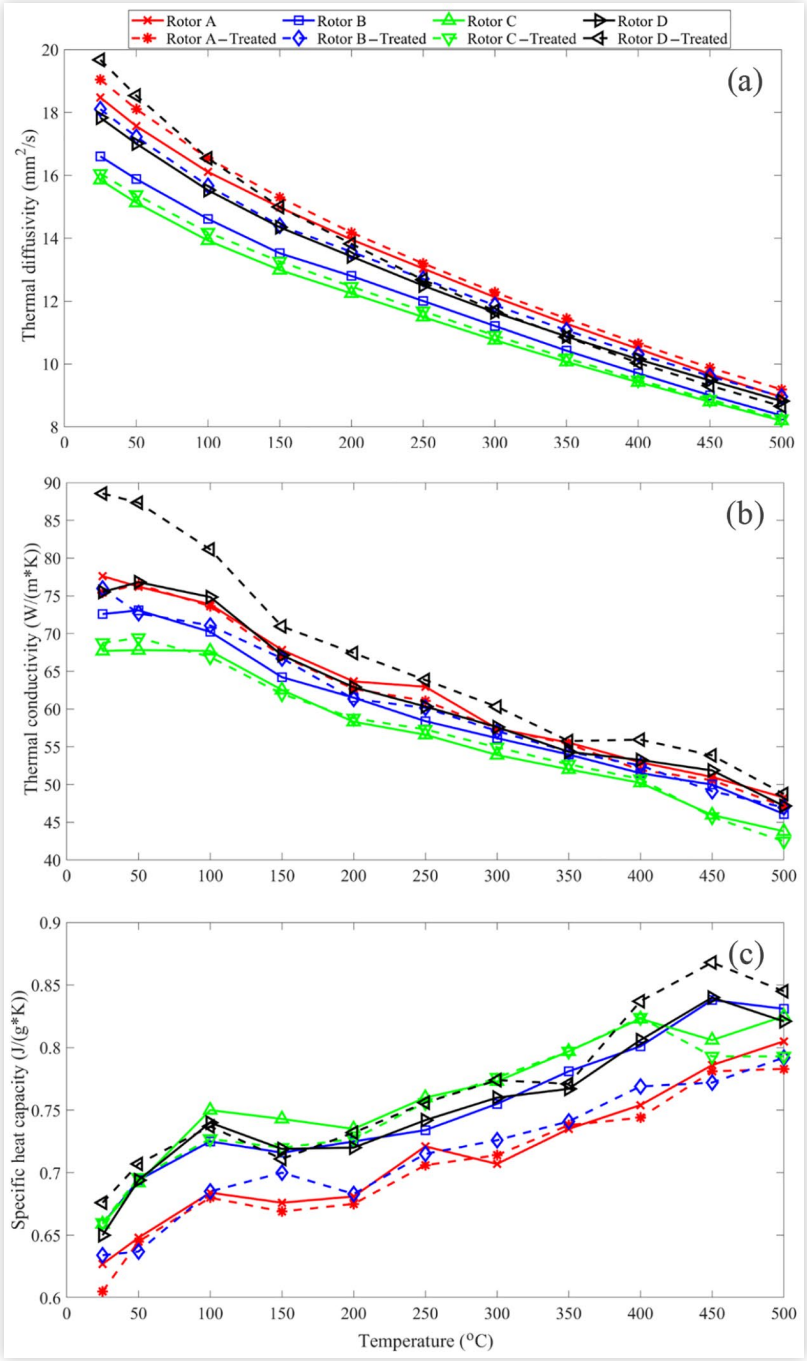




decreased by 1.3%, and for rotors B, C, and D, they were increased by 1.5%, 0.4%, and 7.1%, respectively, when treatment was applied. Contrastingly, specific heat capacities of rotors A, B, and C were approximately decreased by 1.1%, 4.9%, and 1.1%, respectively, and for Rotor D, they were increased by 1.9%. The significant differences observed in the measured thermal properties of the studied rotors could be a result of the microstructural variations identified and the treatment process applied.

In untreated rotors, Rotor A with lower Carbon Equivalent (CE), higher content of graphite, shorter graphite flakes, and lower contents of ferrite and pearlite compared to other selected cast iron types exhibited the highest thermal diffusivities and conductivities. The higher graphite content of Rotor A might have contributed to the high thermal diffusivities and conductivities in untreated rotors, as observed in [23]. However, for specific heat capacities, Rotor C with the lowest graphite content and highest pearlite content exhibited the highest values.

In treated rotors, Rotor D with higher CE, higher ferrite content, and longer graphite flakes compared to other selected cast iron types exhibited the highest thermal diffusivities,

**TABLE 4** Measured thermal diffusivity, thermal conductivity, and specific heat capacity values of untreated and treated rotors at room temperature (25°C) and elevated temperature (500°C).

| | Thermal diffusivity ($mm^2$/sec) | | Thermal conductivity (W/mK) | | Specific heat capacity (J/gK) | |
|---|---|---|---|---|---|---|
| | Room temperature (25°C) | Elevated temperature (500°C) | Room temperature (25°C) | Elevated temperature (500°C) | Room temperature (25°C) | Elevated temperature (500°C) |
| **Untreated rotor A** | 18.5 | 8.9 | 77.6 | 48.3 | 0.63 | 0.81 |
| **Untreated rotor B** | 16.6 | 8.4 | 72.6 | 46.1 | 0.66 | 0.83 |
| **Untreated rotor C** | 15.9 | 8.2 | 67.7 | 43.8 | 0.66 | 0.83 |
| **Untreated rotor D** | 17.8 | 8.8 | 75.5 | 47.2 | 0.65 | 0.82 |
| **Treated rotor A** | 19 | 9.2 | 75.4 | 47.1 | 0.61 | 0.78 |
| **Treated rotor B** | 18.1 | 9 | 76 | 47 | 0.63 | 0.8 |
| **Treated rotor C** | 16.1 | 8.3 | 68.8 | 42.5 | 0.66 | 0.79 |
| **Treated rotor D** | 19.7 | 8.7 | 88.6 | 48.8 | 0.68 | 0.85 |



**TABLE 5** Mathematical regression models of thermal diffusivity, Model 1 and Model 2.

| | Model 1 | | | Model 2 | | |
|---|---|---|---|---|---|---|
| **Parameters** | **Estimate** | **Std. error** | ***p*-value** | **Estimate** | **Std. error** | ***p*-value** |
| **Intercept** | 30.3398 | 1.8895 | 0.000017 | 13.6414 | 0.7469 | 0.000053 |
| **Graphite** | — | — | — | 0.0074 | 0.7470 | 0.0028 |
| **Ferrite** | — | — | — | 0.1221 | 0.0011 | 0.0460 |
| **Pearlite** | −0.0021 | 0.0003 | 0.0013 | — | — | — |
| **Treatment** | 1.0280 | 0.3532 | 0.0334 | 1.0280 | 0.0427 | 0.0385 |
| **Equation** | Thermal diffusivity = (30.3398) + (−0.0021 * Pearlite$^2$) + (−1.028 * Treatment) + Error | | | Thermal diffusivity = (13.6414) + (0.0074 * Graphite$^2$) + (0.1221 * Ferrite$^2$) + (−1.028 * Treatment) + Error | | |
| | **Residual standard error** | | 0.4995 | **Residual standard error** | | 0.4788 |
| | **$R^2$** | | 0.9097 | **$R^2$** | | 0.9336 |



thermal conductivities, and specific heat capacities. The effect of graphite content was not pertinent in the Atomic-Forged® treated rotors, where Rotor D with graphite content lower than Rotor A exhibited higher thermal diffusivities, thermal conductivities, and specific heat capacities. The higher CE, higher contents of ferrite and pearlite, and longer graphite flake sizes of Rotor D, along with the treatment process applied, might have influenced the observed differences in measured thermal properties.

The microstructural characterization of studied rotors along with the treatment process applied has a considerable impact on the measured thermal properties. An increase in graphite content of the studied rotors helped in increasing the thermal diffusivity and thermal conductivity of the bulk material while decreasing the measured specific heat capacity of the same. However, for treated rotors, the influence of graphite content was not dominant compared to the effect of treatment applied. Despite the influence of graphite content and the treatment applied, there may be a combined influence of other microstructural features such as ferrite and pearlite, which may have a significant contribution to the observed thermal properties.

## 4.3. Regression Analysis

To better understand the influence of microstructural differences and the applied treatment process upon the measured thermal properties, three mathematical models using univariate regression analysis were adopted. The models developed in this study include thermal diffusivities, thermal conductivities, and specific heat capacities at measured room temperature as responses, and the contents of graphite, ferrite, pearlite, and treatment of rotors as predictors.

Initial tests have been performed with CE; contents of graphite, ferrite, and pearlite; graphite flake sizes; and measured thermal properties to identify the predictors that resemble reasonable contribution to the developed models. The results from initial tests identified the variables "thermal diffusivity" (or thermal conductivity or specific heat), "graphite" (% volume), "pearlite" (% volume), and "ferrite" (% volume) as quantitative variables, and the variable "treatment" is a categorical variable with two levels, i.e., "Treated" or "Untreated." The dataset used in developing these models consists of eight observations ($n = 8$), i.e., one from each rotor. Models generated contain vital information like estimates (commonly referred to as coefficients), residual standard error, $p$-value, and $R^2$ value, which define the model's ability to predict the required outputs. The model with statistically significant coefficients for all the predictors used, $p$-value of coefficient less than 0.05 (95% confidence), lower residual standard error, and $R^2$ value with comparatively higher accountability for variance, is a good model to predict the required thermal properties. Models with statistically significant However, if the model passes all initial tests, then it is further checked for constant variance using the Breusch-Pagan test. If the $p$-value from the Breusch-Pagan test is

**FIGURE 7** Residual plots for the model with pearlite and treatment (a), for the model with graphite, ferrite, and treatment (b).

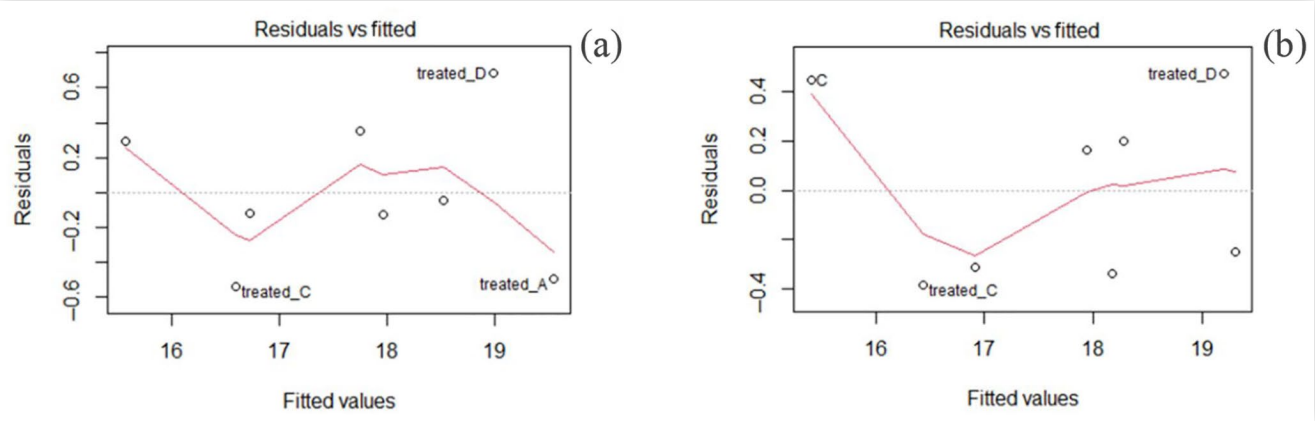




greater than 0.05, then the model predicts values with constant variance. All these statistical techniques helped in developing and validating the below-mentioned models, which take into effect the combined influence of microstructural features and treatment applied, in predicting the required thermal properties.

### 4.3.1. Regression Model of Thermal Diffusivity

The initial verification indicated that perfect multicollinearity exists between pearlite and the other terms of the model, i.e., graphite and ferrite. To overcome this, the model is chosen in such a way that it either includes pearlite or both graphite and ferrite. After several iterations of different models and eliminations using forward and backward elimination approaches, two models were finalized.

1. Model with treatment and second-degree polynomial term of pearlite as predictors (Model 1 in Table 5)
2. Model with treatment and second-degree polynomial terms of graphite and ferrite as predictors (Model 2 in Table 5)

The model that includes graphite ($p$-value = 0.0028), ferrite ($p$-value = 0.0460), and treatment has $p$-values less than 0.05 for each predictor, a slightly better $R^2$ value (0.9336) and residual standard error (0.4788), compared to the model with pearlite ($p$-value = 0.0013) and treatment ($p$-value = 0.0334) with $R^2$ value (0.9097) and residual standard error (0.4995). However, the model with pearlite involves a lower number of predictors and could be considered more feasible in terms of any typical mathematical approach. Despite the influence of microstructural features, the treatment applied had the highest influence in both the models, with a 1.028 estimate coefficient, compared to estimate coefficients of graphite (0.0074), ferrite (0.1221), and pearlite (-0.0021). To better understand the developed models, residuals versus fitted values were plotted, as shown in Figure 7. The lower number of data points available in this study makes it hard to identify any specific pattern in the residual plots generated. In addition to these results, both the models have exhibited constant variance and $p$-values greater than 0.05 as indicated by the Breusch-Pagan test (Table 6). No outliers were detected in the model developed.

To further improve the models, the possibility of transformations was checked on each predictor, but the results did not indicate any real improvements. Based on the results obtained from the statistical approach adopted, it could be deduced that the contents of graphite and ferrite together could have considerable influence over the thermal diffusivity of the bulk material selected. However, the Atomic-Forged® treatment when applied has a higher influence and proves to be dominant over the microstructural differences observed. These statistical results correlate to the findings observed in earlier findings reviewed in this article, where the untreated Rotor A with higher graphite content exhibited higher thermal diffusivity. However, this effect was dominated in treated rotors, where the treated Rotor D, with comparatively lower graphite content than Rotor A, exhibited higher thermal diffusivity.

### 4.3.2. Regression Model of Thermal Conductivity

The $p$-values obtained for the predictors used in the initial model (Table 7 show that graphite with a $p$-value of 0.0473 was significant. However, later investigations, corresponding to individual contributions, found that none of the predictors, alone or in combination, were useful in predicting thermal conductivity ($p$-value > 0.05). Despite the inability to develop a reasonable model, the $R^2$ value generated, given as 0.8021, represents a model with low accountability of variance in predicted values and still shows the existence of a relationship between the predictors used and the response required.

As observed earlier, the graphite content of the bulk material and treatment applied has a considerable impact on thermal conductivity. Despite showing the existence of a relationship between the variables used the data obtained was not

**TABLE 6** Breusch-Pagan test results of models with pearlite and treatment and with graphite, ferrite, and treatment as predictors, respectively.

| Parameters | Model 1 | Model 2 |
|---|---|---|
| **Chi-square** | 0.1286 | 0.4796 |
| **Degrees of freedom** | 1.0000 | 1.0000 |
| ***p*-value** | 0.7199 | 0.4886 |

**TABLE 7** Results of the initial model developed for thermal conductivity with graphite, ferrite, and treatment as predictors.

| | Model 1 | | |
|---|---|---|---|
| **Parameters** | **Estimate** | **Std. error** | ***p*-value** |
| **Intercept** | 39.6678 | 10.7899 | 0.0213 |
| **Graphite** | 1.0694 | 0.3778 | 0.0473 |
| **Ferrite** | 5.0103 | 2.0928 | 0.0748 |
| **Pearlite** | — | — | — |
| **Treatment** | 4.9198 | 2.6775 | 0.1400 |
| **Equation** | Thermal conductivity = (39.6678) + (1.0694 * Graphite) + (5.0103 * Ferrite) + (−4.9198 * Treatment) + Error | | |
| | **Residual standard error** | | 3.7870 |
| | **$R^2$** | | 0.8021 |



**TABLE 8** Results of the initial model developed for specific heat capacity, with graphite, ferrite, and treatment as predictors.

| | Model 1 | | |
|---|---|---|---|
| **Parameters** | **Estimate** | **Std. error** | ***p*-value** |
| **Intercept** | 0.6787 | 0.0594 | 0.0003 |
| **Graphite** | −0.0034 | 0.0021 | 0.1820 |
| **Ferrite** | 0.0132 | 0.0115 | 0.3161 |
| **Pearlite** | — | — | — |
| **Treatment** | 0.0060 | 0.0147 | 0.7049 |
| **Equation** | Specific heat capacity = (0.6787) + (−0.0034 * Graphite) + (0.0132 * Ferrite) + (−0.006 * Treatment) + Error | | |
| | **Residual standard error** | | 0.0209 |
| | **$R^2$** | | 0.5217 |



enough to generate a proper model to help predict the thermal conductivity of the selected bulk material.

**4.3.3. Regression Model of Specific Heat** The *p*-values obtained for the initial model with all the predictors (Table 8) revealed that none of the predictors were useful in predicting specific heat, due to their higher *p*-values. Several models were investigated with individual predictors as well as combinations, but none of them were found to be significant. The $R^2$ value (0.5217) obtained for the initial model (Table 8) corresponds to a poor model with very low accountability of variance in predicting the specific heat capacity values. The model, however, represents a negative influence of graphite content corresponding to the observations made earlier for the measured specific heat capacity, where Rotor C with the least graphite content exhibited the highest specific heat capacity.

The statistical results obtained do not establish a model which could identify the influence of microstructural features and treatment applied. This highlights the need for more statistically relevant data to establish a robust model that can help predict the specific heat capacities of any material with lower variability and higher confidence.

# 5. Conclusions

This work clearly establishes a relationship between the observed microstructural features of studied rotors and the treatment applied on the thermal properties of brake rotors. Mathematical models provide a formal representation of these relationships, which may be important and helpful for the design and optimization of practical braking devices and systems. The following conclusions were drawn based on microstructural features observed, measured thermal properties, and mathematical models generated:

1. Thermal diffusivities and thermal conductivities decrease with increasing temperature, while specific heat capacities increase with increasing temperature.
2. The novel casting/manufacturing process adopted to produce the four studied gray cast irons had considerable influence over the content and morphology of the observed microstructural features. Also the detailed microstructure analysis revealed a good homogeneity of all materials subjected to the modified advanced casting process.
3. The content of graphite had considerable influence over the measured thermal properties of the selected bulk material. Cast iron rotors with higher graphite content helped in increasing the thermal diffusivity and thermal conductivity while reducing the specific heat capacity. A combined effect of graphite and other microstructural features may exist and may contribute significantly toward the thermal properties of the bulk material. Mathematical models to identify this combined influence of different microstructural features observed may play a key role in predicting thermal properties.
4. The treatment process helps in improving the thermal diffusivity of the bulk material. However, its effect is not pertinent over thermal conductivity and specific heat capacity. The microstructural features observed might have a considerable influence over thermal properties, when combined with treatment, and need to be studied using advanced mathematical models.
5. The mathematical models generated help in understanding the combined influence of observed microstructure and treatment over the measured thermal properties. The developed models identify the influence of treatment to be dominant over the content and morphology of graphite, ferrite, and pearlite, in the thermal diffusivity model, with higher estimate coefficients compared to other predictors. However, none of these were found to be contributing well in predicting thermal conductivity and specific heat capacity due to the close overlap of data obtained. The need for more statistically relevant data might help in building new models which can better predict the thermal properties with lower variability and higher confidence.
6. The developed models established a reasonable relationship between graphite content and thermal properties measured that well correlate with the observations made in the preceding parts of this

article. This further highlights the influence of graphite content on the measured thermal properties over any other microstructural feature observed or treatment applied to the cast iron brake rotors.

7. To further improve the accuracy of the models in predicting the thermal properties, the measurement of more statistically relevant experimental data is recommended for future work.

## Acknowledgments

The authors would like to gratefully acknowledge Dr. Darshan Ravoori for assistance in the thermal property measurements and Mr. Matthew Schultz from Waupaca Foundry Inc. for assistance in the chemical analysis of the studied rotors.

## Contact Information

Correspondence: rohit.jogineedi@siu.edu
Tel.: +1-618-353-4800
Department of MEEP, 1230 Lincoln Drive, Carbondale, IL 62901, USA

## References

1. ASTM A48/A48M-03, *Standard Specification for Gray Iron Castings* (West Conshohocken, PA: ASTM International, 2012)
2. Japanese Industrial Standards Committee, *JIS G 5501—Grey Iron Castings* (Japan: Standards Association, 1995)
3. Cho, M. et al., "Tribological Study of Gray Cast Iron with Automotive Brake Linings: The Effect of Rotor Microstructure," *Tribology International* 36, no. 7 (2003): 537-545.
4. Davis, J.R., *ASM Specialty Handbook: Cast Irons* (Materials Park, OH: ASM International, 1996)
5. Allain, S.B.Y. et al., "Microstructure-Based Behavior Law for Globular Pearlitic Steels," *Journal of Materials Research and Technology* 8, no. 3 (2019): 3373-3376.
6. ASTM, *Standard Test Method for Evaluating the Microstructure of Graphite in Iron Castings* (West Conshohocken, PA: ASTM International, 2010)
7. Lu, H. et al., "Effects of Different Graphite Types on the Thermal Fatigue Behavior of Bionic Laser-Processed Gray Cast Iron," *Metallurgical and Materials Transactions A* 49, no. 11 (2018): 5848-5857.
8. Wang, G. et al., "Effects of Inoculation on the Pearlitic Gray Cast Iron with High Thermal Conductivity and Tensile Strength," *Materials* 11, no. 10 (2018): 1876.
9. Liu, Y. et al., "Effect of Graphite Morphology on the Tensile Strength and Thermal Conductivity of Cast Iron," *Materials Characterization* 144 (2018): 155-165.
10. Collini, L., Nicoletto, G., and Konečná, R., "Microstructure and Mechanical Properties of Pearlitic Gray Cast Iron," *Materials Science and Engineering: A* 488, no. 1-2 (2008): 529-539.
11. Benedetti, M., Fontanari, V., and Lusuardi, D., "Effect of Graphite Morphology on the Fatigue and Fracture Resistance of Ferritic Ductile Cast Iron," *Engineering Fracture Mechanics* 206 (2019): 427-441.
12. Plume, G. and Rousseau, C.-E., "Spall Behavior of Cast Iron with Varying Microstructures," *Journal of Applied Physics* 116, no. 3 (2014): 034903.
13. Chen, J. and Chen, S., "On Thermal Conductivity of an In-Situ Metal Matrix Composite-Cast Iron," in Intech Open, *Metal, Ceramic and Polymeric Composites for Various Uses* (IntechOpen Limited, United Kingdom, 2011), 211.
14. Ajeel, S.A. and Hasoni, S.M., "Ductile and Gray Cast Irons Deterioration with Time in Various NaCl Salt Concentrations," *Engineering and Technology Journal* 26, no. 2 (2008): 154-168.
15. Rhee, S.K., DuCharme, R., and Spurgeon, W.M., "Characterization of Cast Iron Friction Surfaces," SAE Technical Paper 720056, 1972, https://doi.org/10.4271/720056.
16. Filip, P., "Friction and Wear of Polymer Matrix Composite Materials for Automotive Braking Industry," in *Braking 2002. From the Driver to the Road. Papers from the International Conference*, Leeds, United Kingdom, 2002.
17. Anderson, A.E., *Friction and Wear of Automotive Brakes* (Materials Park, OH: ASM International, 1992)
18. Hee, K. and Filip, P., "Performance of Ceramic Enhanced Phenolic Matrix Brake Lining Materials for Automotive Brake Linings," *Wear* 259, no. 7-12 (2005): 1088-1096.
19. Filip, P., Weiss, Z., and Rafaja, D., "On Friction Layer Formation in Polymer Matrix Composite Materials for Brake Applications," *Wear* 252, no. 3-4 (2002): 189-198.
20. Handa, Y. and Kato, T., "Effects of Cu Powder, $BaSO_4$ and Cashew Dust on the Wear and Friction Characteristics of Automotive Brake Pads," *Tribology Transactions* 39, no. 2 (1996): 346-353.
21. Anderson, A. and Knapp, R., "Hot Spotting in Automotive Friction Systems," *Wear of Materials* 1989, no. 2 (1989): 673-680.
22. Bashir, M., Qayoum, A., and Saleem, S., "Analysis of Frictional Heating and Thermal Expansion in a Disc Brake Using COMSOL," *Journal of Physics: Conference Series* 1240 (2019): 012094.
23. Hecht, R.L., Dinwiddie, R.B., and Wang, H., "The Effect of Graphite Flake Morphology on the Thermal Diffusivity of Gray Cast Irons Used for Automotive Brake Discs," *Journal of Materials Science* 34, no. 19 (1999): 4775-4781.
24. Bai, Y. et al., "Chemical Compositions, Microstructure and Mechanical Properties of Roll Core Used Ductile Iron in Centrifugal Casting Composite Rolls," *Journal of Materials Science & Technology* 28, no. 9 (2012): 853-858.
25. Wang, G.-Q. et al., "Effects of Alloying Elements on Thermal Conductivity of Pearlitic Gray Cast Iron," *Journal of Iron and Steel Research International* 26, no. 9 (2019): 1022-1030.
26. Maluf, O. et al., "Effect of Alloying Elements on Thermal Diffusivity of Gray Cast Iron Used in Automotive Brake Disks," *Journal of Materials Engineering and Performance* 18, no. 7 (2009): 980-984.
27. Moonesan, M. and Madah, F., "Effect of Alloying Elements on Thermal Shock Resistance of Gray Cast Iron," *Journal of Alloys and Compounds* 520 (2012): 226-231.

28. Karthikayan, S. et al., "Innovative Research Trends in the Application of Thermal Barrier Metal Coating in Internal Combustion Engines," *Materials Today: Proceedings* 4, no. 8 (2017): 9004-9012.
29. Yin, Z. et al., "Microstructure and Mechanical Properties of $Al_2O_3$-Al Composite Coatings Deposited by Plasma Spraying," *Applied Surface Science* 254, no. 6 (2008): 1636-1643.
30. Wadsworth, I. et al., "Thermal Stability and Oxidation Resistance of TiAlN/CrN Multilayer Coatings," *Surface and Coatings Technology* 94 (1997): 315-321.
31. PalDey, S. and Deevi, S., "Single Layer and Multilayer Wear Resistant Coatings of (Ti, Al) N: A Review," *Materials Science and Engineering: A* 342, no. 1-2 (2003): 58-79.
32. Sahraoui, T. et al., "Structure and Wear Behaviour of HVOF Sprayed $Cr_3C_2$-NiCr and WC-Co Coatings," *Materials & Design* 24, no. 5 (2003): 309-313.
33. Toma, D., Brandl, W., and Marginean, G., "Wear and Corrosion Behaviour of Thermally Sprayed Cermet Coatings," *Surface and Coatings Technology* 138, no. 2-3 (2001): 149-158.
34. Xie, M., Zhang, S., and Li, M., "Comparative Investigation on HVOF Sprayed Carbide-Based Coatings," *Applied Surface Science* 273 (2013): 799-805.
35. Ampaw, E. et al., "Carbonitriding 'Pack Cyaniding' of Ductile Irons," *Advanced Materials Research* 1132 (2016): 330-348.
36. Pang, H. et al., "Condensed Matter: Structure, Mechanical and Thermal Properties: Microstructure and Corrosion Performance of Carbonitriding Layers on Cast Iron by Plasma Electrolytic Carbonitriding," *Chinese Physics Letters* 26, no. 8 (2009): 086805.
37. Holly, M.L., DeVoe, L., and Webster, J., "Ferritic Nitrocarburized Brake Rotors," SAE Technical Paper 2011-01-0567, 2011, https://doi.org/10.4271/2011-01-0567.
38. Tlili, S. and Touhami, M.Z., "Enhancement of the Mechanical Properties of Graycast Iron by Ferritic Nitrocarburizing Process," in *Congrès Algérien de la Mécanique CAM*, 2011.
39. Filip, P. and Meckel, N.K., Wear resistant braking systems. Google Patents, 2021.
40. Chatterjee, S. and Hadi, A.S., *Regression Analysis by Example* (Somerset: John Wiley & Sons, 2015)
41. Cook, R.D. and Weisberg, S., *Residuals and Influence in Regression* (New York: Chapman and Hall, 1982)
42. Breusch, T.S. and Pagan, A.R., "A Simple Test for Heteroscedasticity and Random Coefficient Variation," *Econometrica: Journal of the Econometric Society* (1979): 1287-1294.
43. Mansfield, E.R. and Helms, B.P., "Detecting Multicollinearity," *The American Statistician* 36, no. 3a (1982): 158-160.
44. Armstrong, R.A., "When to Use the Bonferroni Correction," *Ophthalmic and Physiological Optics* 34, no. 5 (2014): 502-508.
45. Fox, J. and Weisberg, S., *An R Companion to Applied Regression* (Thousand Oaks, CA: Sage Publications, 2018)
46. Parker, W. et al., "Flash Method of Determining Thermal Diffusivity, Heat Capacity, and Thermal Conductivity," *Journal of Applied Physics* 32, no. 9 (1961): 1679-1684.
47. Cape, J. and Lehman, G., "Temperature and Finite Pulse-Time Effects in the Flash Method for Measuring Thermal Diffusivity," *Journal of Applied Physics* 34, no. 7 (1963): 1909-1913.
48. Sen, A. and Srivastava, M., "Multiple Regression," in: *Regression Analysis* (New York: Springer, 1990), 28-59.
49. Razaq, A. et al., "Influence of Alloying Elements Sn and Ti on the Microstructure and Mechanical Properties of Gray Cast Iron," *Procedia Manufacturing* 37 (2019): 353-359.
50. Gonzaga, R. et al., "Mechanical Properties Dependency of the Pearlite Content of Ductile Irons," *Journal of Achievements in Materials and Manufacturing Engineering* 33, no. 2 (2009): 150-158.




ISSN 0148-7191